Available online at www.sciencedirect.com
ScienceDirect
International Journal of Heat and Fluid Flow 29 (2008) 352–363
International Journal of HEAT AND FLUID FLOW
www.elsevier.com/locate/ijhff

# Effects of pass arrangement and optimization of design parameters on the thermal performance of a multi-pass heat exchanger

Min-Soo Kim, Kwan-Soo Lee *, Simon Song

*School of Mechanical Engineering, Hanyang University, 17 Haengdang-dong, Seongdong-gu, Seoul 133-791, Republic of Korea*

Received 18 November 2006; received in revised form 30 May 2007; accepted 30 May 2007
Available online 12 July 2007

**Abstract**

This paper presents a numerical evaluation of the flow distribution and thermal performance of a multi-pass, multi-channel heat exchanger as functions of the number of passes and inlet diameter. To determine the optimal number of passes for a fixed size of heat exchanger, we investigated the JF factor by varying the number of passes and the inlet diameter. We determined the optimal number of passes for a given inlet diameter by studying the variation of the JF factor as a function of the ratio of the inlet diameter to header height ratio. For instance, the optimal number of passes was two for an inlet diameter of 50 mm, and the performance based on the JF factor was improved by about 89% compared to a reference heat exchanger. We further optimized other design parameters, such as the inlet location, separator location, and header width to improve the heat exchanger performance by an additional 20%.


*Keywords:* Multi-pass heat exchanger; Number of passes; Optimization; Response surface method

## 1. Introduction

Multi-channel, parallel-flow heat exchangers are frequently used in refrigeration and air-conditioning systems to maximize their efficiency and minimize their volume. However, a key issue with the multi-channel, parallel-flow heat exchanger is the non-uniformity of the pressure and flow distributions between the channels inside the heat exchanger block. This decreases the thermal performance and increases the pressure drop across the heat exchanger, reducing the overall performance. In addition, the non-uniformity causes local hot spots in the heat exchanger, that reduce its life span. Therefore, it is important to study the characteristics of the flow distribution and the thermal performance inside the heat exchanger block as well as its fin-side characteristics (Missirlis et al., 2005).

Several studies (Choi et al., 1993; Jiao et al., 2003; Lalot et al., 1999; Lee and Oh, 2004) have investigated design parameters such as the header shape, ratio of header area to channel area, channel length, and locations of the inlet and outlet, since they affect the flow distribution inside the heat exchanger and its thermal performance. These studies have proposed various methods to improve the flow distribution uniformity and the performance of the heat exchanger, but were limited to single-pass, multi-channel heat exchangers with a dividing and combining header. Recent multi-channel heat exchangers tend to have multiple passes, repeatedly dividing and combining the flow in order to obtain a high thermal performance and flow distribution uniformity for a given system volume (Maharudrayya et al., 2006). Therefore, it is necessary to investigate the characteristics of the flow distribution inside the heat exchanger block and the effects of design parameters on the performance of a multi-pass, multi-channel heat exchangers.

There are few studies of multi-pass, multi-channel heat exchangers. Nakamura et al. (1989) proposed a multi-block method to obtain a uniform flow distribution in a power charger with multiple passes. Strictly speaking, however, the heat exchanger they used was not a multi-pass one

* Corresponding author. Tel.: +82 2 2220 0426; fax: +82 2 2295 9021.
*E-mail address:* ksleehy@hanyang.ac.kr (K.-S. Lee).

0142-727X/$ - see front matter © 2007 Elsevier Inc. All rights reserved.
doi:10.1016/j.ijheatfluidflow.2007.05.010

**Nomenclature**

| | |
|---|---|
| $C_{1-2}$, $C_\mu$ | turbulence constants |
| $C_p$ | specific heat at a constant pressure |
| $D$ | inlet diameter [mm] |
| $d$ | channel spacing [mm] |
| $e$ | relative error |
| $f_i$ | body force of gravity |
| $G_k$ | generation of turbulence kinetic energy |
| $H$ | header height [mm] |
| JF | JF factor |
| $k$ | thermal conductivity [W/mK] |
| $k$ | turbulence kinetic energy [$m^2/s^2$] |
| $\dot{m}$ | flow rate [kg/s] |
| $N$ | number |
| $N_{i,ch}$ | channels number of $i$ pass |
| $n$ | normal direction |
| $p$ | pressure [Pa] |
| $S$ | flow uniformity |
| $T$ | temperature [°C] |
| $u$ | velocity [m/s] |
| $w$ | header width [mm] |
| $X$ | design parameter |
| $x$ | normalized design parameter |

*Greek symbols*

| | |
|---|---|
| $\Delta$ | difference |
| $\delta_{ij}$ | Kronecker delta |
| $\varepsilon$ | turbulence kinetic energy dissipation rate [$m^2/s^3$] |
| $\mu$ | dynamic viscosity [kg/m s] |
| $\rho$ | density [$kg/m^3$] |
| $\sigma_k$, $\sigma_\varepsilon$ | turbulent Prandtl number of $k$, $\varepsilon$ |
| $\Phi$ | dependent variable |

*Subscripts*

| | |
|---|---|
| c | channel |
| eff | effective |
| f | fluid |
| ideal | ideal case |
| max | maximum |
| min | minimum |
| new | present |
| old | previous |
| ref | reference |
| s | solid |
| t | turbulence |

because the combining headers had their own outlets. Chung et al. (2002) investigated the characteristics of the flow distribution and optimized the performance of a four-pass, parallel-flow heat exchanger by examining the number of channels per pass and the inlet and outlet locations. Rao and Das (2004) studied the thermal performance of a multi-pass, plate heat exchanger, although the number of passes was restricted to two or three. They did not report the flow characteristics in each pass, and did not examine how the number of passes affects the flow distribution and overall performance. Further study is therefore required on how the number of passes affects the performance of multi-pass heat exchangers.

This paper addresses the effects of various design parameters, including the number of passes and the inlet diameter, on the performance of a multi-pass heat exchanger. We propose an optimal multi-pass, multi-channel heat exchanger for a fixed system volume based on a simultaneous evaluation of the flow distribution and thermal performance. In addition, we optimize other design parameters, such as the locations of the inlet and the pass separator, and the header width, to improve the performance of the heat exchanger with an optimal number of passes.

## 2. Heat exchanger geometry and mathematical formulation

The heat exchanger in this study consists of outside fins and a multi-pass, multi-channel heat exchanger block, as shown in Fig. 1. The heat is transferred through a 2-mm thick wall between the fins and the block. The fin length, height and thickness are fixed at 240, 50, and 0.5 mm, respectively, and there are 83 fins. The fin, separator, and other solid walls are all made of aluminum. The fins cool high-temperature air that flows between the fins. The inside of the heat exchanger block consists of a variable number of passes. The circular inlet and outlet are located at the center of the first and last headers, respectively. Each pass has multiple channels spaced at 10-mm intervals. The channel wall is 0.5-mm thick. In the multi-pass heat exchanger block, the low-temperature fluid introduced through the inlet is divided amongst all the channels in the dividing header and is combined in the combining header. This process is repeated in each pass until the fluid leaves the heat exchanger at an elevated temperature. In this paper, each channel is denoted by channel $i$–$j$, where index $i$ indicates the pass number and index $j$ indicates the channel number in the pass. The channel numbers are ordered from the top to the bottom of a pass.

To examine the effects of the number of passes on the heat exchanger performance, we considered several models, shown in Fig. 2. The reference model has two passes and an inlet diameter of 30 mm, other models have the same configuration as the reference model in terms of overall size, channel spacing, header width, outside fins, and so on, but the number of passes and the location of the separators differ. The number of passes is an even number, since the locations of the inlet and outlet are restricted to the right-hand side of the heat exchanger; this is given as a

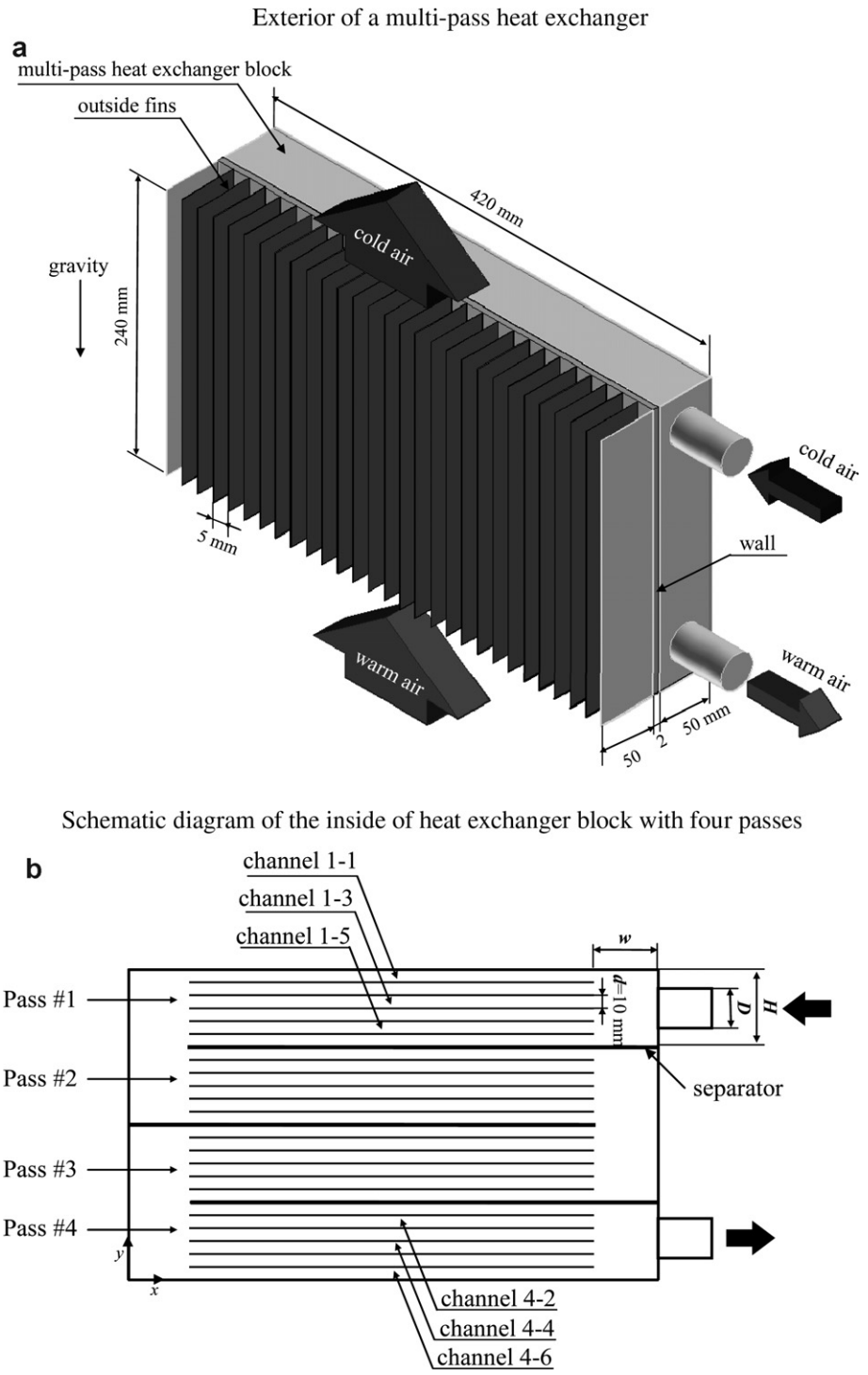


Fig. 1. Schematic diagram of a typical multi-pass, multi-channel heat exchanger.

design limitation. Each pass in any model has the same number of channels.

### 2.1. Governing equations

For our numerical analysis of the heat exchanger models, we assumed the following:

(1) The flows in the heat exchanger are three-dimensional, steady, incompressible, and turbulent.
(2) The working fluid is a single phase, and the fluid properties remain constant based on the operational temperature given in Eqs. (11) and (12).
(3) The thermal contact resistance is negligible between solid walls.

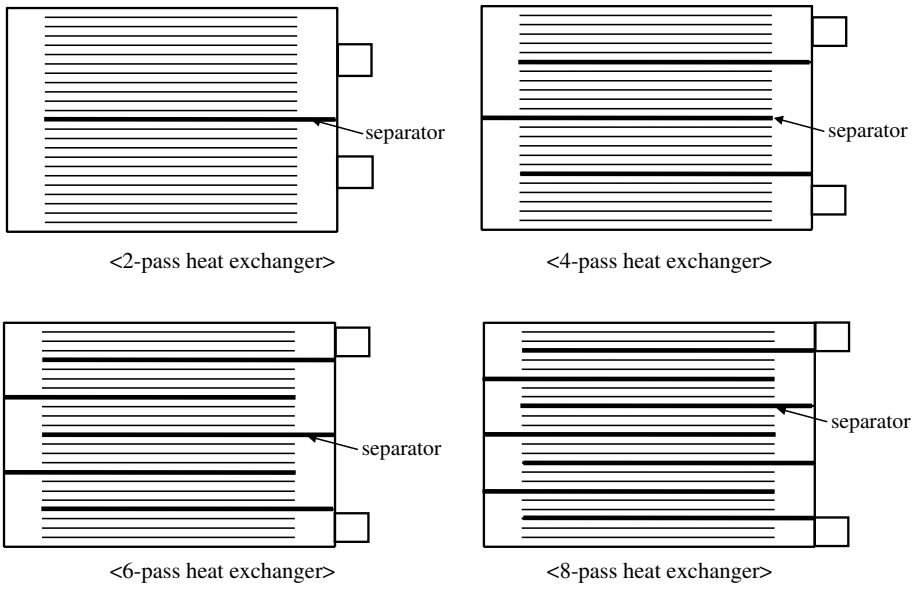


Fig. 2. Various pass arrangements for a heat exchanger (with an inlet diameter of 30 mm).

To ensure that the flow is fully-developed at the inlet, we added a computational domain to the inlet which is a 10 times longer pipe than the inlet hydraulic diameter. Since the flows are fully developed turbulent at the inlet according to the Reynolds number based on the hydraulic diameter and inlet velocity, the standard $k$–$\varepsilon$ model was used for the numerical calculations. Therefore, the governing equations for the fluid regions consist of the continuity, momentum, $k$–$\varepsilon$, and energy equations as follows:

The continuity equation:

$$\frac{\partial}{\partial x_i}(\rho u_i) = 0 \tag{1}$$

The momentum equation:

$$\frac{\partial}{\partial x_j}(\rho u_i u_j) = -\frac{\partial p}{\partial x_i} + \frac{\partial}{\partial x_j}\left[(\mu + \mu_t)\frac{\partial u_i}{\partial x_j}\right] + \rho f_i \tag{2}$$

The $k$-equation:

$$\frac{\partial}{\partial x_j}(\rho u_j k) = \frac{\partial}{\partial x_j}\left[\left(\mu + \frac{\mu_t}{\sigma_k}\right)\frac{\partial k}{\partial x_j}\right] + G_k - \rho\varepsilon \tag{3}$$

The $\varepsilon$-equation:

$$\frac{\partial}{\partial x_j}(\rho u_j \varepsilon) = \frac{\partial}{\partial x_j}\left[\left(\mu + \frac{\mu_t}{\sigma_\varepsilon}\right)\frac{\partial \varepsilon}{\partial x_j}\right] + C_1 G_k \frac{\varepsilon}{k} - C_2 \rho \frac{\varepsilon^2}{k} \tag{4}$$

The energy equation:

$$\rho C_p \frac{\partial}{\partial x_j}(u_j T) = k_{\text{eff}} \frac{\partial^2 T}{\partial x_j^2} + (\tau_{ij})_{\text{eff}} \frac{\partial u_i}{\partial x_j} \tag{5}$$

where

$$\mu_t = \rho C_\mu \frac{k^2}{\varepsilon} \tag{6}$$

$$G_k = 2\mu_t S_{ij} S_{ij} = \mu_t \left(\frac{\partial u_j}{\partial x_i} + \frac{\partial u_i}{\partial x_j}\right)\frac{\partial u_i}{\partial x_j} \tag{7}$$

$$C_1 = 1.44, \quad C_2 = 1.92, \quad C_\mu = 0.09, \quad \sigma_k = 1.0, \quad \sigma_\varepsilon = 1.3 \tag{8}$$

$$(\tau_{ij})_{\text{eff}} = \mu_{\text{eff}}\left(\frac{\partial u_j}{\partial x_i} + \frac{\partial u_i}{\partial x_j}\right) - \frac{2}{3}\mu_{\text{eff}}\frac{\partial u_i}{\partial x_i}\delta_{ij}, \quad k_{\text{eff}} = k_f + \frac{C_p \mu_t}{\text{Pr}_t}, \quad \mu_{\text{eff}} = \mu + \frac{\mu_t}{0.9} \tag{9}$$

Wall function was used near the walls where the dependent variables had large gradients.

For the solid wall, the following conduction equation was used:

$$k_s \frac{\partial^2 T}{\partial x_j^2} = 0 \tag{10}$$

The boundary condition (Costa et al., 1999) for the air at the inlet of the outside fins was

$$\dot{m} = \dot{m}_{\text{in}} = 0.02115\ \text{kg/s}, \quad k_{\text{in}} = 0.01 u_{\text{in}}^2, \quad \varepsilon_{\text{in}} = \frac{C_\mu k_{\text{in}}^{1.5}}{0.05 D_{\text{in}}}, \quad T_f = T_{\text{in}} = 5\ ^\circ\text{C} \tag{11}$$

The inlet boundary condition for the interior of the heat exchanger block was

$$\dot{m} = \dot{m}_{\text{in}} = 0.004\ \text{kg/s}, \quad k_{\text{in}} = 0.01 u_{\text{in}}^2, \quad \varepsilon_{\text{in}} = \frac{C_\mu k_{\text{in}}^{1.5}}{0.05 D_{\text{in}}}, \quad T_f = T_{\text{in}} = -30\ ^\circ\text{C} \tag{12}$$

The outlet boundary conditions for the flow were

$$\dot{m} = \dot{m}_{\text{out}} = \dot{m}_{\text{in}}, \quad \frac{\partial k}{\partial n} = 0, \quad \frac{\partial \varepsilon}{\partial n} = 0, \quad \frac{\partial p}{\partial n} = 0, \quad \frac{\partial T}{\partial n} = 0 \tag{13}$$

On the solid walls, the boundary conditions are given as

$$u_{\text{wall}} = v_{\text{wall}} = w_{\text{wall}} = 0 \tag{14}$$

$$T_f = T_s, \quad k_f \frac{\partial T_f}{\partial n} = k_s \frac{\partial T_s}{\partial n} \tag{15}$$

### 2.2. Numerical method and validation

We used the FLUENT software package to simulate the flow of fluid in the multi-pass heat exchanger. We selected the SIMPLE algorithm to couple the velocity and pressure. To improve the accuracy, we applied a second-order upwind scheme to the convective terms of the governing equations. In addition, we tested the grid dependence of the calculations by varying the number of grids in each channel, as shown in Fig. 3. After considering the accuracy, convergence, and computation time, we selected a grid structure consisting of 1,161,216 subdivisions. More grids were placed near the walls for better accuracy, as shown in Fig. 4. The convergence criterion was the relative error of the dependent variables defined in Eq. (16). The criterion is $10^{-6}$ for all of the equations. The computation time was 20 h using a 3.0 GHz Pentium IV processor.

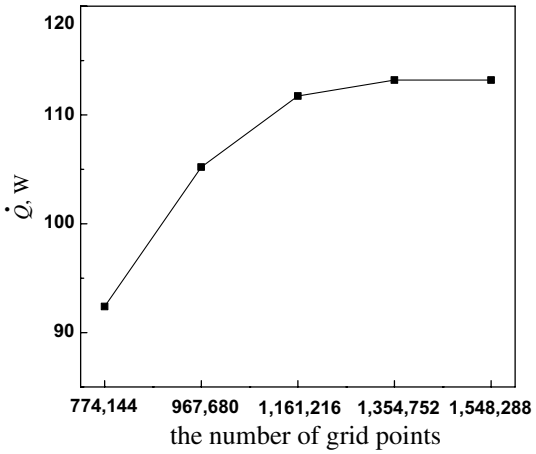


Fig. 3. Grid dependence as a function of the number of points.

Table 1
Comparison of the heat transfer rate with experimental data

| Model | $\dot{Q}$ (W) | Relative error (%) |
|---|---|---|
| Experiment[a] | 115 | – |
| Standard $k$–$\varepsilon$ | 111.75 | 2.826 |
| RNG $k$–$\varepsilon$ | 110.85 | 3.609 |
| Lam and Bremhost | 106.72 | 7.2 |

[a] This was performed by the manufacturer of the heat exchangers of interest.

$$e = \mathrm{Max}\left[\left|\frac{\Phi_{\mathrm{new}} - \Phi_{\mathrm{old}}}{\Phi_{\mathrm{new}}}\right|\right] \tag{16}$$

The results of the standard $k$–$\varepsilon$ model were compared with the experimental results provided by the manufacturer of the heat exchanger as well as the results of the RNG $k$–$\varepsilon$ and low-Re Lam and Bremhost $k$–$\varepsilon$ model (Lam and Bremhost, 1981). The all flow geometries for the comparison are identical to the geometry shown in Fig. 1b. We performed the numerical simulations using the same flow and temperature conditions given in Eqs. (11) and (12). For the low-Reynolds model, the local $y+$ values were less than 1.0, more grid points in comparison with the standard $k$–$\varepsilon$ model (Missirlis et al., 2005). However the grids for the low-Reynolds model could not be made finer because of CPU speed and computational time limitations. Thus we selected the standard $k$–$\varepsilon$ model whose results agreed well with the experimental data as shown in Table 1.

## 3. Results and discussion

We performed numerical analyses to investigate the performance of multi-pass, multi-channel heat exchangers by varying the number of passes and inlet diameter. After selecting a model with the optimal number of passes and

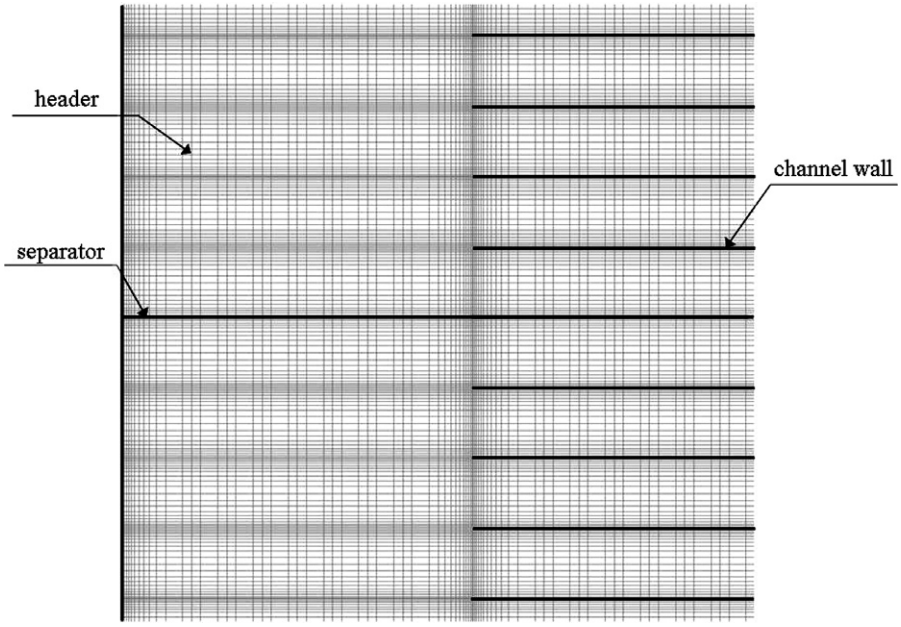


Fig. 4. Details of the grid near the header.

inlet diameter, we examined the effects and sensitivity of other design parameters on the performance. The design parameters we studied were the inlet and outlet locations, the header width, and the separator location.

### 3.1. Effects of the number of passes and the inlet diameter

To investigate the effects of the inlet diameter on the performance of the heat exchanger, we varied the diameter from 20 to 50 mm at 5-mm intervals. The outlet diameter was set to be the same as the inlet diameter. We also varied the number of passes; this was an even number (e.g., 2, 4, 6, 8, or 12) because the locations of the inlet and outlet were restricted to the right-hand side of the heat exchanger. The maximum number of passes was determined by the inlet diameter since the overall size of the heat exchanger was fixed.

The JF factor (Lee and Oh, 2004; Yun and Lee, 2000) was used to evaluate the performance of the heat exchanger model. The results are summarized in Table 2. For a given number of passes, the JF factor increased as the inlet diameter increased since the pressure drop between the inlet and the outlet decreased as without significantly changing the heat transfer rate. For example, the heat transfer rate for the four-pass heat exchanger varied slightly from 111 to 112 W as the inlet diameter increased, but the pressure drop decreased significantly from 104 to 14 Pa. Therefore, the overall performance of the heat exchanger was best when the inlet diameter was 50 mm for the given range of inlet diameter.

More passes resulted in a greater heat transfer rate but a larger pressure drop for a fixed inlet diameter. Fig. 5 shows the pressure distribution in the dividing and combining headers on the first pass of a heat exchanger with the inlet diameter of 30 mm. For the two-pass heat exchanger, there was a significant pressure drop along the middle channels between the dividing and combining headers, while the pressure drop was negligible along outer channels since the inlet diameter was small compared to the header height of 120 mm. As a result, the majority of the fluid flowed through the middle channels, leading to a low heat transfer rate. As the number of passes increased up to eight, the pressure distribution became more uniform, improving both the uniformity of the flow and the heat transfer rate. However, the overall pressure drop between the inlet and the outlet increased as the number of passes increased. The change in the heat transfer rate (larger was better) and the pressure drop (smaller was better) tended to offset each other since they both increased with the number of passes. For inlet diameters of 20, 30, and 50 mm, the number of passes that resulted in the best performance was six, four, and two respectively, as shown in Table 2.

We considered the ratio of the inlet diameter to the header height ($D/H$) as a variable to determine the optimal number of passes since the header height depended on the number of passes, and was equal to the pass height, as shown in Fig. 2. Fig. 6 shows the effects of this ratio on the JF factor. It was greatest when the ratio was in the range of 0.25–0.5, regardless of the inlet diameter. For large inlet diameters, there were

Table 2
Performance of heat exchangers as a function of the inlet diameter and number of passes

| Inlet diameter (mm) | Number of passes ($N_p$) | $D/H$ | $\dot{Q}$ (W) | $\Delta p$ (Pa) | JF |
|---|---|---|---|---|---|
| 20 | 2 | 0.167 | 104.30 | 99.04 | 0.537 |
| | 4 | 0.333 | 111.70 | 103.51 | 0.616 |
| | 6 | 0.5 | 117.65 | 122.23 | 0.640 |
| | 8 | 0.667 | 121.03 | 201.64 | 0.583 |
| | 12 | 1 | 124.86 | 610.42 | 0.494 |
| 25 | 2 | 0.208 | 103.44 | 37.00 | 0.761 |
| | 4 | 0.417 | 111.72 | 45.65 | 0.841 |
| | 6 | 0.625 | 117.25 | 68.84 | 0.791 |
| | 8 | 0.833 | 120.99 | 150.02 | 0.780 |
| 30 | 2[a] | 0.25 | 104.24 | 18.63 | 1 |
| | 4 | 0.5 | 111.75 | 27.09 | 1.022 |
| | 6 | 0.75 | 117.38 | 51.18 | 0.882 |
| | 8 | 1 | 120.80 | 134.11 | 0.710 |
| 35 | 2 | 0.292 | 104.20 | 10.61 | 1.245 |
| | 4 | 0.583 | 111.35 | 19.33 | 1.180 |
| | 6 | 0.875 | 116.61 | 49.92 | 0.910 |
| 40 | 2 | 0.333 | 104.55 | 6.87 | 1.517 |
| | 4 | 0.667 | 111.96 | 15.76 | 1.322 |
| | 6 | 1 | 116.38 | 49.89 | 0.938 |
| 45 | 2 | 0.375 | 105.47 | 5.11 | 1.749 |
| | 4 | 0.75 | 112.41 | 14.30 | 1.356 |
| 50 | 2 | 0.417 | 106.45 | 4.20 | 1.893 |
| | 4 | 0.833 | 112.37 | 13.74 | 1.385 |

[a] Reference heat exchanger.

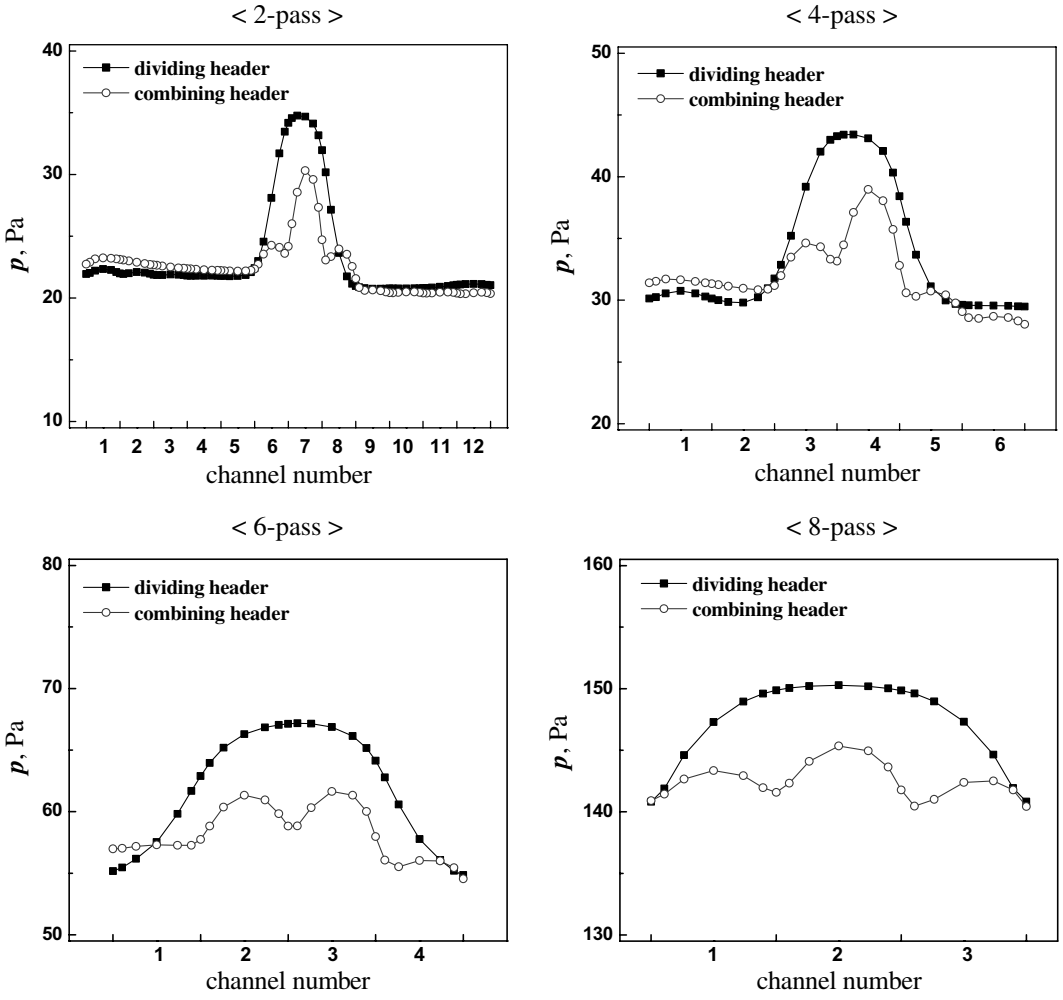


Fig. 5. Pressure distribution at each header on the first pass as a function of the channel number and number of passes for an inlet diameter of 30 mm.

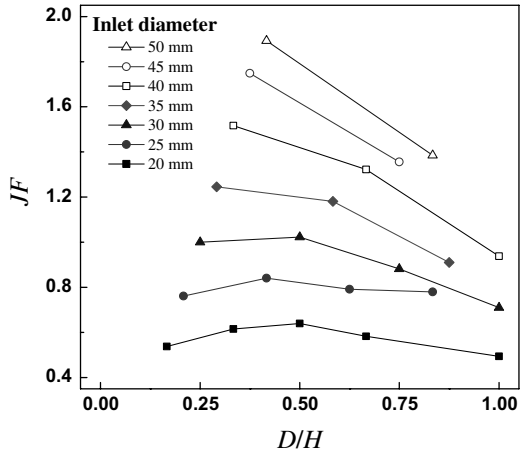


Fig. 6. JF factor as a function of the ratio of the inlet diameter to the header height.

few discrete values for this ratio, but and they were all close to 0.5 because the number of passes was constrained to an even number while the inlet diameter varied from 20 to 50 mm at 5-mm intervals and the size of the heat exchangers was fixed. Thus, it is reasonable to conclude that the optimal number of passes was dictated by the inlet diameter when the value of $D/H$ was approximately 0.5. For example, from Table 2, the optimal number of passes was four for an inlet diameter of 30 mm. Overall, the heat exchanger with the largest JF factor had an inlet diameter of 50 mm and two passes, and the performance was 89.3% higher than that of the reference heat exchanger.

### 3.2. Effect and sensitivity of the design parameters

We investigated the effects of other design parameters on the performance of the two-pass heat exchanger with the largest JF factor. These parameters were the locations of the inlet, outlet, and separator, as well as the header width, as shown in Fig. 7. They varied within set geometrical limitations, shown in Table 3, and were normalized to the upper ($X_{i,\max}$) and lower ($X_{i,\min}$) limits of the constraint conditions of each parameter as follows:

$$x_i = \frac{X_i - X_{i,\mathrm{ref}}}{\frac{1}{2}(X_{i,\max} - X_{i,\min})} \tag{17}$$

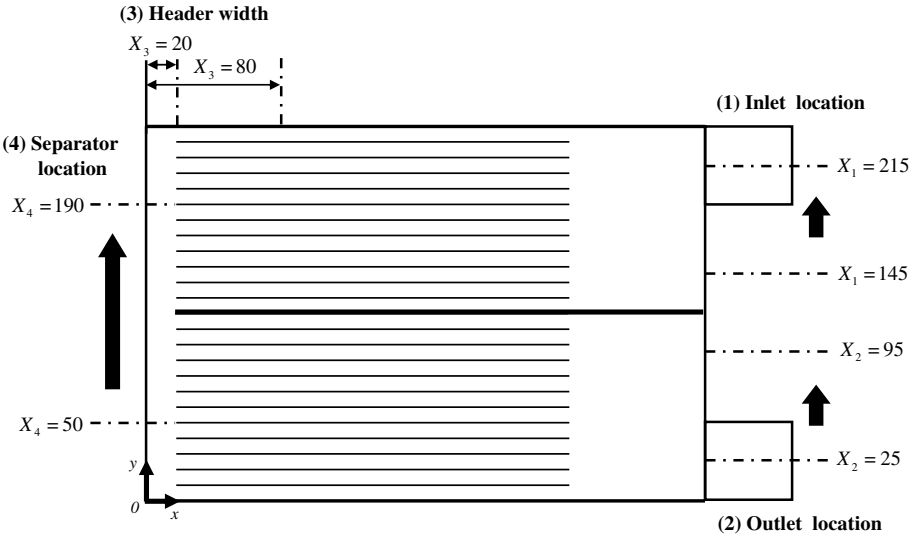


Fig. 7. Ranges of the design parameters.

Table 3
Ranges of the normalized design parameters

| Design parameter | Normalization (mm) | | |
|---|---|---|---|
| | −1 (lower) | 0 (reference) | +1 (upper) |
| Inlet location ($X_1$) | 145 | 180 | 215 |
| Outlet location ($X_2$) | 25 | 60 | 95 |
| Left header width ($X_3$) | 20 | 50 | 80 |
| Separator location ($X_4$) | 50 | 120 | 190 |

While one design parameter was varied, the other normalized parameters were fixed to a reference value of zero.

Fig. 8 shows the JF factor and the uniformity of the flow distribution with respect to the inlet locations. Because the heat exchanger consisted of two passes, the flow distribution uniformity could be defined as

$$S_{\text{total}} = \sqrt{\left\{ \sum_{i=1}^{2} \sum_{j=1}^{N_{i,\text{ch}}} \left( \frac{\dot{m}_{i,j} - \dot{m}_{i,\text{ideal}}}{\dot{m}_{i,\text{ideal}}} \right)^2 \right\} \Big/ N_{\text{c}}} \tag{18}$$

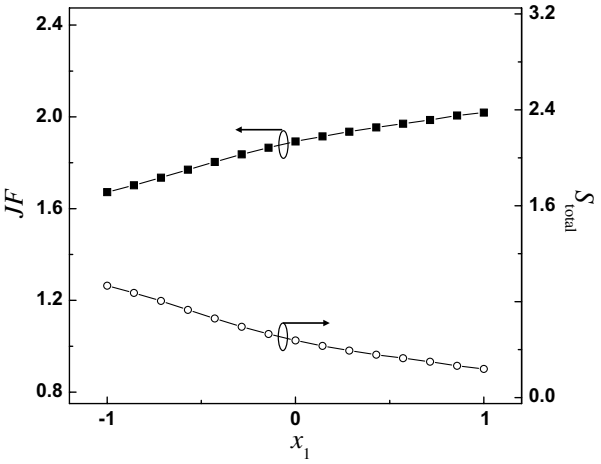


Fig. 8. JF factor and flow distribution uniformity as a function of the inlet location.

where the subscripts $i$ and $j$ indicate the pass and channel number, respectively, and $N_{\text{c}}$ is the total number of channels in the heat exchanger. More uniform flows gave a smaller value of $S_{\text{total}}$. As the inlet location moved toward the top of the exchanger, the JF factor increased and $S_{\text{total}}$ decreased, indicating that the performance of the heat exchanger improved. A comparison of the pressure distributions in the headers on the first pass indicated that the improved performance resulted from an increased flow uniformity, as shown in Fig. 9. For the lowest inlet location ($x_1 = -1$), the pressure drop along the upper channels was so small that the fluid hardly flowed through them. However, it was significantly higher in the lower channels. In the combining header of the first pass, the fluids moved down perpendicular to the channels. Therefore, the local momentum increased and the local pressure decreased as the flows combined in the header (Bahura and Jones, 1976). This caused a higher pressure drop along the lower channels. As the inlet location moved upward, the pressure drop along the channels became more uniform so that the flow was distributed more evenly, thus improving the heat transfer performance. The increase in the JF factor was therefore due to the improved flow uniformity as the inlet location moved upward.

Fig. 10 shows the variation of the JF factor for the other three design parameters. As the outlet location moved upward from $x_2 = -1$, the JF factor increased until $x_2 = -0.57$ ($X_2 = 40$ mm), and then decreased. This is because the pressure drop decreased until $x_2 = -0.57$ but increased sharply thereafter, while the heat transfer rate increased slowly throughout, proportional to the change in outlet location.

The header width also significantly affected the flow distribution and thus the overall heat exchanger performance. The left header width varied from 20 to 80 mm with respect to the fixed left side wall. Since the channel length remained at 320 mm, the relative channel position shifted to the

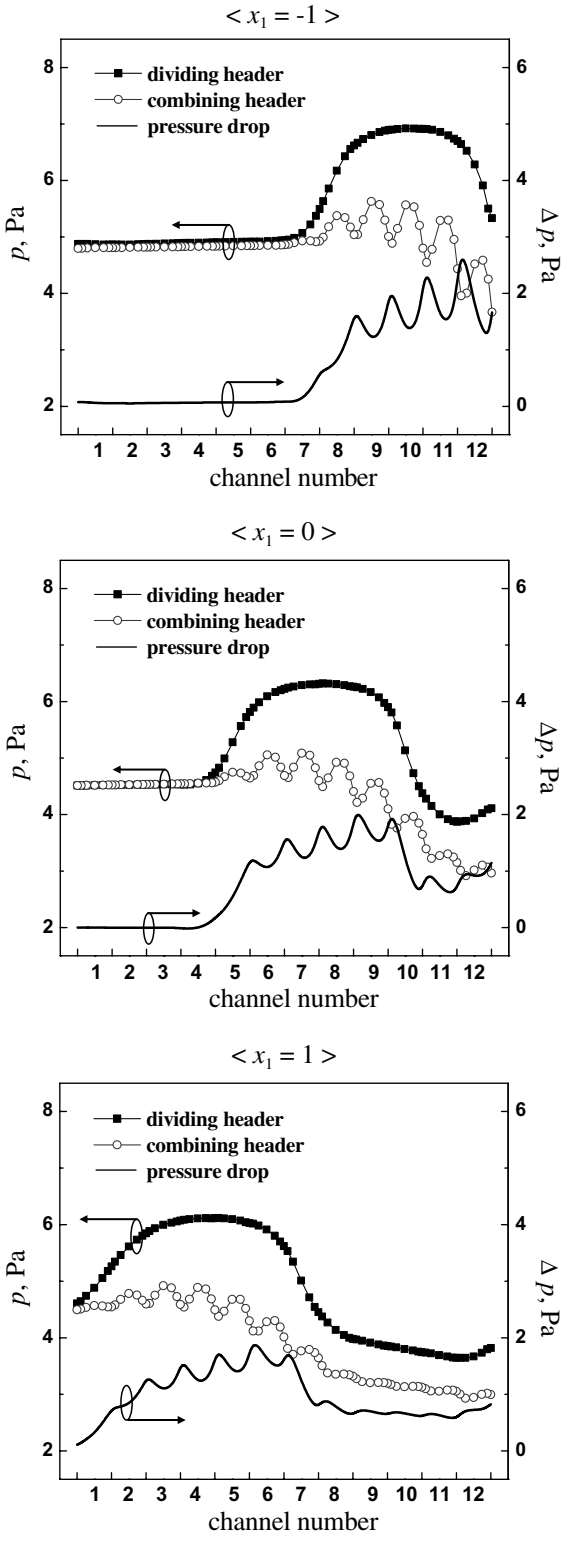


Fig. 9. Pressure distribution at each header on the first pass as a function of the inlet location.

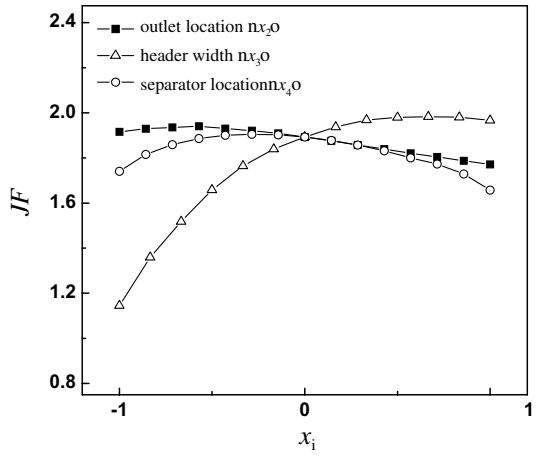


Fig. 10. JF factor as a function of outlet location, header width, and separator location.

right, reducing the width of the right headers. Thus for an increased width of the left header, the widths of the combining header for the first pass and the dividing header for the second pass increased, while the widths of the dividing header for the first pass and the combining header for the second pass decreased. As the header width varied from $x_3 = -1$ to $x_3 = 0.67$ ($X_3 = 70$ mm), the JF factor increased dramatically, and then changed only slightly for higher values. This is because the flow distribution improved significantly up to $x_3 = 0.67$.

As the separator location moved upward, the JF factor increased for $x_4 = -1$ to $x_4 = -0.28$ ($X_4 = 100$ mm), and decreased gradually thereafter. When the separator location was biased toward either the top or the bottom, the pass with fewer channels showed better flow uniformity, although the results are omitted here for simplicity. However, the overall flow uniformity was best when the separator was located near the middle of the heat exchanger.

In order to examine the flow uniformity and verify the results of Fig. 8, we defined the ratio of the flow rate in a channel to the total flow rate in a pass as follows:

$$\mathrm{FR}\ (\%) = \frac{\dot{m}_i}{\sum_{i=1}^{n} \dot{m}_i} \times 100 \tag{19}$$

where the numerator is the flow rate in a channel, and the denominator is the total flow rate of a pass. For a left header width of 20 mm, most flows were biased to the lower channels (the channels with the greater numbers), as shown in Fig. 11. This is because the header was too narrow and, consequently, it caused a severely non-uniform pressure drop across the channels. The negative flow rates in the upper channels were caused by back flows due to a recirculation zone in the upper corner of the combining header. For a left header width of 50 mm, the uniformity improved slightly compared to the previous case, especially in the first pass. In contrast, for the largest header width ($X_3 = 80$ mm), most fluids flowed through the middle channels. The overall flow distribution in both passes was best for a header width of $X_3 = 80$ mm.

The flow non-uniformity shown in Fig. 11 was worse in the second pass than in the first. Fig. 12 shows the pressure

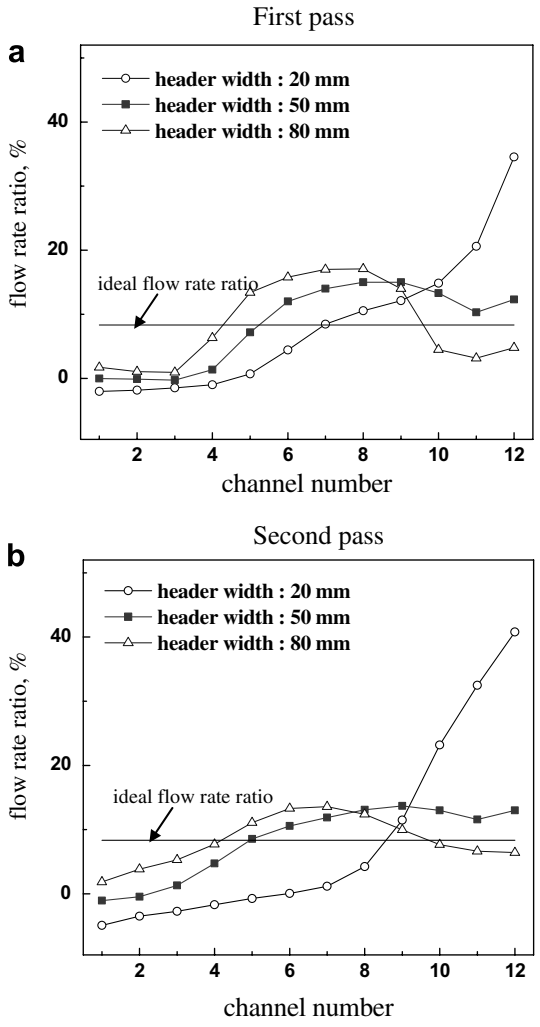


Fig. 11. Flow rate ratios between channels as a function of the header width.

distributions in the first and second passes. Significant pressure differences are observed only along the lower channels of the first and second passes. If the flows from the lower channels of the first pass entered into the upper channels of the second pass, they should have made a sharp turn to enter the upper channels in the second pass, resulting in a significant loss. This is probably a reason that the flows are biased toward the lower channels of the second pass.

Table 4
Sensitivity of the design parameters

| Content | Range (mm) | JF factor | | Difference | Order |
|---|---|---|---|---|---|
| | | Max | Min | | |
| Inlet location | 145–215 | 2.018 | 1.672 | 0.346 | 2 |
| Outlet location | 25–95 | 1.941 | 1.771 | 0.170 | 4 |
| Left header width | 20–80 | 1.983 | 1.145 | 0.838 | 1 |
| Separator location | 50–190 | 1.905 | 1.657 | 0.248 | 3 |

After investigating the effects of the four design parameters on the heat exchanger performance, we examined the sensitivities of the parameters using the difference between the maximum and minimum values of the JF factor shown in Table 4. In decreasing order of importance, the parameters with the greatest effects on performance were the header width, inlet location, separator location, and outlet location. Therefore, we removed outlet location from consideration for the optimization in the next section.

## 4. Optimization

We selected the inlet location ($x_1$), header width ($x_3$), and separator location ($x_4$) as design variables for the optimization. The following optimum design problem was defined considering an objective function and constraint conditions:

$$\begin{aligned} &\text{Find} && x_1, x_3, x_4 \\ &\text{to maximize} && \mathrm{JF}(x_1, x_3, x_4) \\ &\text{subject to} && x_1 - 2x_4 + 1 \geqslant 0 \end{aligned} \tag{20}$$

Experimental points for optimization were selected using a central composite design to create a response surface. A second-order polynomial was used to estimate the

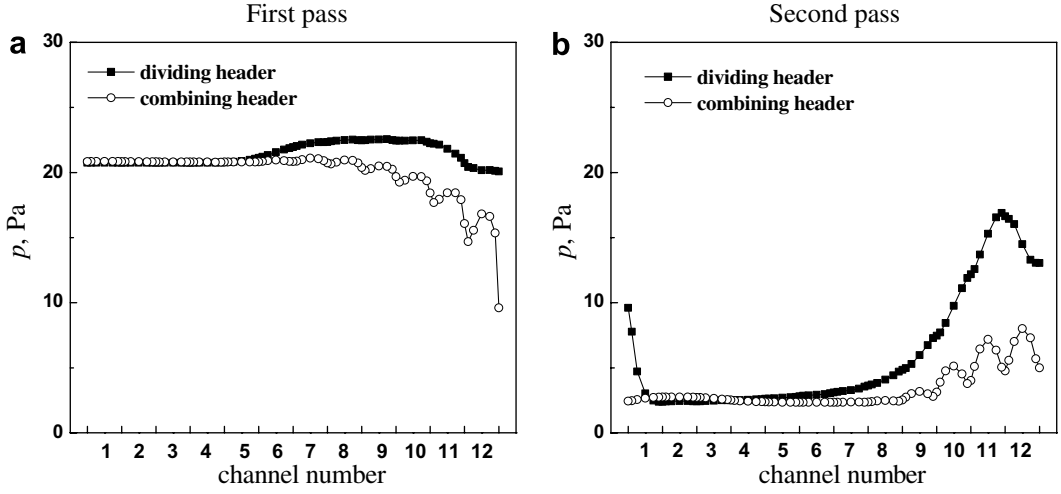


Fig. 12. Pressure distribution at each header for a left header width of 20 mm.

Table 5
Design of experiments

| Test number | Normalization units | | | JF factor |
|---|---|---|---|---|
| | $x_3$ | $x_1$ | $x_4$ | |
| 1 | −1 | −1 | −1 | 1.236 |
| 2 | 1 | −1 | −1 | 1.924 |
| 3 | −1 | 1 | −1 | 1.058 |
| 4 | 1 | 1 | −1 | 1.570 |
| 5 | −1 | −1 | 1 | Violated |
| 6 | 1 | −1 | 1 | Violated |
| 7 | −1 | 1 | 1 | 1.042 |
| 8 | 1 | 1 | 1 | 1.588 |
| 9 | −1 | 0 | 0 | 1.145 |
| 10 | 1 | 0 | 0 | 1.967 |
| 11 | 0 | −1 | 0 | 1.672 |
| 12 | 0 | 1 | 0 | 2.018 |
| 13 | 0 | 0 | −1 | 1.731 |
| 14 | 0 | 0 | 1 | Violated |
| 15 | 0 | 0 | 0 | 1.893 |

full quadratic model for the response surface. The 15 experimental points obtained from the central composite design are shown in Table 5. Based on the experimental points, the following response surface was generated using the objective function and constraint conditions:

$$\begin{aligned} \mathrm{JF}(x_1, x_3, x_4) = {} & 1.8607 + 0.3427x_3 + 0.1730x_1 \\ & - 0.3035x_4 - 0.2966x_3^2 - 0.0076x_1^2 \\ & - 0.4170x_4^2 - 0.0611x_3x_1 \\ & + 0.0256x_3x_4 + 0.3060x_1x_4 \end{aligned} \quad (21)$$

An analysis of variance (ANOVA) was performed to validate the accuracy of the response surface, and the coefficient of determination ($R^2$) was 0.989. Based on Eq. (21), the optimal point was determined as

$$x_1 = 1.0, \quad x_3 = 0.5, \quad x_4 = 0.0 \quad (22)$$

These results indicate that the optimal inlet location, header width, and separator locations were 215, 65, and 120 mm respectively. At that design point, the value of the JF factor was 2.093, meaning that the performance of this optimum model was 109% better than the reference model.

## 5. Conclusions

We conducted a numerical investigation of the performance of a multi-pass, multi-channel heat exchanger considering the number of passes and inlet diameter. After determining optimum number of passes and the inlet diameter, we evaluated the heat exchanger performance by varying the header width, and the locations of the separator, inlet, and outlet. We optimized these to achieve the best performance.

The heat transfer rate varied slightly as the inlet diameter increased for a fixed number of passes while the pressure drop decreased dramatically, improving the overall performance of the heat exchanger. For a fixed inlet diameter, both the heat transfer rate and the pressure drop increased as the number of passes increased. Therefore, the optimum number of passes was different for different inlet diameters, and was determined based on the ratio of inlet diameter to header height of 0.5.

For the heat exchanger with the optimal number of passes and inlet diameter, the design parameters with the greatest effect on performance were, in decreasing order, the header width, inlet location, separator location, and outlet location. After a sensitivity test, the first three design parameters were selected for optimization. The optimization using a response surface a model of which the performance was 109% better than the reference heat exchanger.

In summary, the selection of the optimal number of passes and inlet diameter resulted in a performance 89% better than the reference model. Optimization of other design parameters led to an additional 20% improvement in the performance of the heat exchanger. This shows that the proper choice of the number of passes and the inlet diameter of a multi-pass, and multi-channel heat exchanger are critical can dramatically improve its performance.

## Acknowledgement

This work was supported by the research fund of Hanyang University (HY-2005-I) and the Center of Innovative Design Optimization Technology (iDOT), Korea Science and Engineering Foundation.

## References

Bahura, R.A., Jones, E.H., 1976. Flow distribution manifolds. Journal of Fluids engineering 98, 654–666.

Choi, S.H., Shin, S., Cho, Y.I., 1993. The effect of area ratio on the flow distribution in liquid cooling module manifolds for electronic packaging. International communications in heat and mass transfer 20 (2), 221–234.

Chung, K., Lee, K.S., Kim, W.S., 2002. Optimization of the design factors for thermal performance of a parallel-flow heat exchanger. International Journal of Heat and Mass Transfer 45 (24), 4773–4780.

Costa, J.J., Oliveira, A., Blay, D., 1999. Test of several versions for the $k$–$\varepsilon$ type turbulence modeling of internal mixed convection flows. International Journal of Heat and Mass Transfer 42 (23), 4391–4409.

Jiao, A., Zhang, R., Jeong, S., 2003. Experimental investigation of header configuration on flow maldistribution in plate-fin heat exchanger. Applied Thermal Engineering 23 (10), 1235–1246.

Lalot, S., Florent, P., Lang, S.K., Bergles, A.E., 1999. Flow maldistribution in heat exchangers. Applied Thermal Engineering 19 (8), 847–863.

Lam, C.K.G., Bremhost, K., 1981. A modified form of the $k$–$\varepsilon$ model for prediction wall turbulence. Journal of Fluid Engineering-Transactions of the ASME 103, 456–460.

Lee, K.S., Oh, S.J., 2004. Optimal shape of the multi-passage branching system in a single-phase parallel-flow heat exchanger. International Journal of Refrigeration 27 (1), 82–88.

Maharudrayya, S., Jayanti, S., Deshpande, A.P., 2006. Pressure drop and flow distribution in multiple parallel-channel configurations used in proton-exchange membrane fuel cell stacks. Journal of Power Sources 157 (1), 358–367.

Missirlis, D., Yakinthos, K., Palikaras, A., Katheder, K., Goulas, A., 2005. Experimental and numerical investigation of the flow field through a heat exchanger for aero-engine applications. International Journal of Heat and Fluid Flow 26, 440–458.

Nakamura, Y., Jia, W., Yasuhara, M., 1989. Incompressible flow through multiple passages. Numerical Heat Transfer Part A 16, 451–465.

Rao, B.P., Das, S.K., 2004. Effects of flow distribution to the channels on the thermal performance of the multipass plate heat exchangers. Heat Transfer Engineering 25 (8), 48–59.

Yun, J.Y., Lee, K.S., 2000. Influence of design parameters on the heat transfer and flow friction characteristics of the heat exchanger with slit fins. International Journal of Heat and Mass Transfer 43 (14), 2529–2539.